Received: 30 June 2022 | Revised: 18 October 2022 | Accepted: 23 November 2022

DOI: 10.1002/jrs.6478

RESEARCH ARTICLE

Journal of RAMAN SPECTROSCOPY WILEY

# Development of a Raman spectroscopy system for in situ monitoring of microwave-assisted inorganic transformations

**John Jamboretz**[1] | **Andreas Reitz**[1] | **Christina S. Birkel**[1,2]

[1]School of Molecular Sciences, Arizona State University, Tempe, Arizona, USA

[2]Technische Universität Darmstadt, Darmstadt, Germany

**Correspondence**
Christina Birkel, Technische Universität Darmstadt, Darmstadt 64287, Germany.
Email: christina.birkel@asu.edu

**Funding information**
Deutsche Forschungsgemeinschaft, Grant/Award Number: 456639820; National Science Foundation, Grant/Award Number: 2143982

## Abstract

Microwave heating methods offer unique advantages in preparations of inorganic solids due to the high heating rates, potentially selective heating, and time/energy reductions. Understanding of these enhancements as well as involved mechanisms is poor due to the lack of available and easily applicable in situ monitoring methods, particularly for samples in the solid state. Existing in situ studies typically rely on access to beamline facilities as well as custom-built microwave systems, which is in the best case inconvenient and in the worst case not achievable. In situ Raman spectroscopy is an ideal technique as it provides rapid and unambiguous phase identification by a noncontact method. Further, the instrument components are simple and compact, facilitating use in the typical synthetic laboratory. Only a few reports on using Raman spectroscopy for in situ measurements during microwave heating exist, and they all utilize specialized custom reactor setups. In this work, a new Raman measurement system designed to observe inorganic transformations in situ that is readily deployable in a standard, commercially available laboratory scale microwave reactor is described. As a simple demonstration, the anatase-to-rutile phase transition in $TiO_2$ is monitored under both microwave and conventional furnace heating. The excellent time resolution achieved demonstrates the utility of the system in understanding microwave-assisted methods for the preparation of inorganic compounds. The simplicity will encourage integration by the non-specialist to understand microwave heating for synthetic preparations and promote wider application of the technique.

**KEYWORDS**

inorganic compounds, microwave heating, nonconventional synthesis, phase transformation, Raman spectroscopy, Titania

## 1 | INTRODUCTION

Nonconventional microwave heating has been increasingly adopted for the preparation of inorganic materials.[1–3] In microwave heating, electromagnetic radiation is directly converted to thermal energy within the material and/or a secondary susceptor, whereas conventional (furnace) heating relies on propagation of thermal energy from external sources such as resistive heating elements. Comparatively, microwaves permit extremely rapid heating rates (>1000°C/min, e.g., rapid heating of amorphous carbon)[4,5] and potentially selective heating of reactants, unlocking novel syntheses and microstructural control. This commonly provides significant reductions in processing times and energy usage compared with conventional heating methods.[2] This has been widely demonstrated for the synthesis of a plethora of inorganic solids, such as carbides (e.g., SiC), chalcogenides (e.g., PbSe and ZnS), and oxides (e.g., $CuFe_2O_4$).[4–14] Despite the fact that microwave heating has been used for the synthesis/processing of solid materials since the early 1990s (roughly 30 years, see respective review articles),[4,5,15,16] significant difficulties still exist in the monitoring and control of this novel method.

In situ monitoring of chemical changes is of crucial importance in the control of microwave processing and gaining understanding of possible enhancements. Various in situ monitoring techniques have been explored to study microwave heating of solids; these include X-ray diffraction,[17–22] neutron diffraction,[23–25] dielectric properties measurement,[26] and Raman spectroscopy.[18,27,28] Although these have yielded very interesting insights into the fundamental differences of microwave heating compared with conventional methods, they are limited in their ease of adoption. The X-ray and neutron scattering studies utilize beam line facilities (introducing obvious limitations in time) with the exception of the work published by Robb et al.[22] This, to our knowledge, is the only such study using a laboratory scale X-ray diffractometer, and despite restricting the 2θ angles analyzed to 41–48°, a slow heating rate of 1 $K\,min^{-1}$ was necessary to achieve good time/temperature resolution due to the low X-ray flux rendering the method impractical for rapidly heated samples. The dielectric property measurement apparatus proposed by Catala-Civera et al.[29] and subsequently used to study microwave heating of various materials by Garcia-Baños et al.[26] is especially insightful as these properties dictate the efficiency in converting microwave radiation to heat.[1,2,4] These properties could be monitored in real time for even complex mixtures. The custom-built apparatus is technically complex, however, and ill-suited to the non-specialist. In fact, all studies referenced here rely on custom microwave applicator designs presenting a significant barrier in adoption.

Raman spectroscopy is a uniquely suited technique for in situ studies of microwave heating of inorganics. It probes the vibrational energy levels in solids and molecules by collecting inelastically scattered photons from a monochromatic excitation source (e.g., a laser). The technique provides noncontact and generally unambiguous phase identification in Raman active solids.[30] Furthermore, a host of other chemical and physical properties can be derived by a more detailed analysis, including temperature, composition, nanosizing, and strain.[31–39] In particular, the simple and compact instrumentation allow wider deployment in the basic synthetic laboratory environment.

A few studies have successfully employed Raman spectroscopy to study microwave heating of solids.[18,27,28] The Raman apparatus presented by Tompsett et al.[18] utilizes a custom probe of quartz, a microwave compatible material, which could enter the custom microwave applicator through a machined access slot in the waveguide. The probe was used to study the formation of zeolites in solution at temperatures of up to 130°C. The Raman data derived showed only diminishing signals from the precursor solution and no definitive signals indicating product formation, which the authors attribute to the increasing opacity of the solution. Its operation at higher temperatures or on condensed phases was not demonstrated. Vaucher et al.[27] demonstrated in situ Raman spectroscopic monitoring of microwave heating of a diamond/silicon mixture. Their apparatus utilized a standard Raman probe microscope objective that could access the sample surface through a slot in the custom microwave applicator above the sample surface. Deriving the temperature from the Raman data collected showed evidence of selective heating of the silicon over the diamond by the microwave radiation. They additionally utilized the apparatus to study the conversion of magnetite ($Fe_3O_4$) to hematite ($Fe_2O_3$) by microwave heating. Garcia-Baños et al.[28] utilized a standard Raman probe in their custom dual-mode microwave heating/dielectric properties measurement system. They monitored the Raman shift associated with temperature-induced phase transitions in bismuth titanate ($Bi_4Ti_3O_{12}$) and potassium sulfate ($K_2SO_4$) to calibrate the measured surface temperature to presumed bulk temperature based on the known temperatures of these conversions. The results of these studies all demonstrate the potential for Raman spectroscopic monitoring under microwave heating conditions. However, as in the other in situ techniques described, these all use specialized custom microwave reactors. None are specifically designed for or demonstrated in standard

commercially available reactors, presenting a serious barrier in adoption.

This motivated the development of a new kind of Raman probe and measurement system for studying solid-state transformations in typical laboratory scale microwave reactors. The system incorporates a new probe design with a long working distance (15 cm) and completely microwave compatible materials. It is specifically designed to be readily incorporated into commercial laboratory microwaves that have a top-mounted through-hole access port of suitable dimensions to permit the probe. The measurement system is further optimized for the study of solid-state transformations at high temperatures by utilizing a confocal optical design and raster scanning.

As a proof-of-concept, the well-known anatase-to-rutile phase transition in $TiO_2$[40] was observed under both conventional (furnace) and microwave heating methods at temperatures exceeding 800°C. These results demonstrate the feasibility of the new probe and measurement system developed to observe inorganic transformations. They also clearly show the utility of in situ Raman spectroscopy in the study of microwave heating methods for inorganic compounds, which remain poorly understood, and compare these directly with conventional heating methods. Special considerations in the design of the system are discussed.

## 2 | INSTRUMENT DESIGN

The new Raman measurement system was specifically designed to be usable in commercially available laboratory microwave reactors, such as the Mars 6 Synthesis microwave (CEM) used in this work. The microwave reactor must include a microwave field-blocking access port at the top of the reactor with a minimum diameter of ~50 mm for this probe design. The entire instrument schematic and photograph with major components labeled is presented in Figure 1.

The custom Raman probe (Figure 2a) is 30 cm in length allowing it to enter the microwave chamber through an access port at the top and place the objective lens close to the sample while keeping the remaining optics outside of the reactor. It accepts common 1-inch (25.4 mm) diameter optics, which are secured in place by a length of internal threading and lock rings. The external termination of the probe has standard external C-mount threading that allows coupling to customizable optics. Alumina was selected as the material because it is microwave transparent and mechanically stiff.[41] The probe was custom manufactured (Ortech Ceramics).

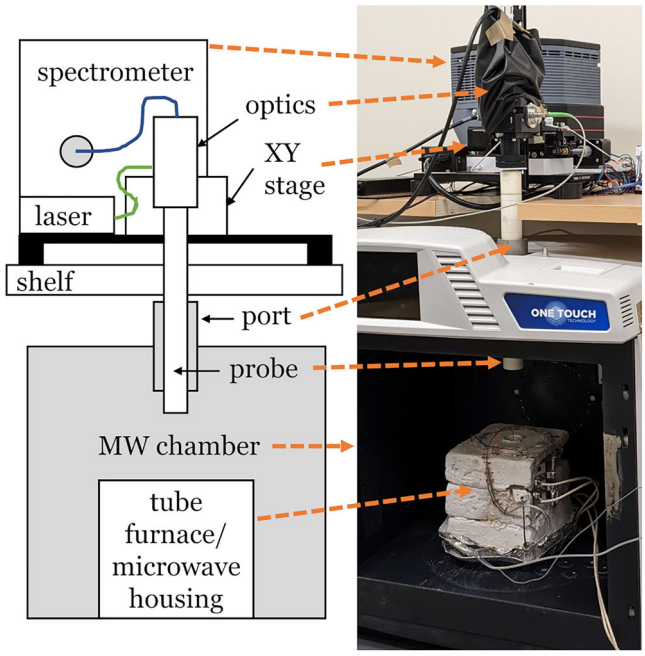


FIGURE 1 Schematic and photograph of entire system with major components labeled. Photograph is with tube furnace installed. [Colour figure can be viewed at wileyonlinelibrary.com]

The optical path including all components is shown in Figure 2b. A laser (532 nm CW, 100 mW, Samba 100, Hübner Photonics) is delivered by fiber optic to an adjustable aspheric collimator (PAF2P-18A, Thorlabs) that provides a ~3 mm diameter beam. The beam is passed through a cleanup filter (Teledyne Princeton Instruments) and is reflected 90° by a dichroic (Teledyne Princeton Instruments) to the objective lens (AC254-150-A, Thorlabs). The objective lens acts to both focus the laser on the sample and collimates the collected Raman signal in a standard backscattering configuration. The laser spot size is ~31 μm minimum at perfect focus on the sample surface. As focusing is performed at the beginning of the experiment and remains unchanged, the actual size is likely larger due to changing distance between sample and objective during experiments (i.e., sample and support expansion/contraction).

Note that this objective lens is the only optic within the microwave reactor. The glass components are not expected to couple (heat) strongly with the microwave irradiation. The cement used between the lenses of the doublet and antireflective coating material is unknown. However, no significant degradation in performance during strong (1000 W) microwave irradiation or between numerous conventional or microwave experiments has been observed. This suggests persistent thermal damage to the lens is not significant with this particular lens, focal length, physical arrangement, and experimental temperatures. Transient changes in performance during

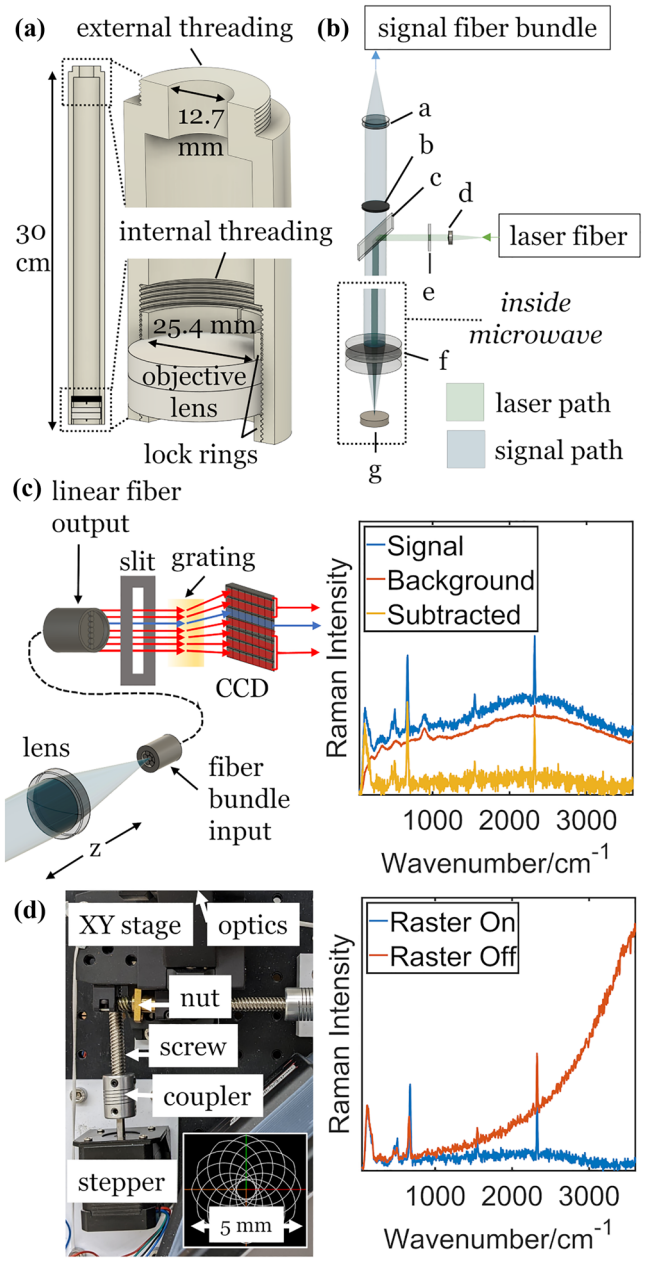


**FIGURE 2** (a) Raman probe schematic. (b) Optical path schematic. a: Signal fiber lens; b: edge filter; c: dichroic filter; d: laser collimator lens; e: laser line filter; f: objective lens; g: sample. The break in the optical path indicates the length of the Raman probe. (c) Left: schematic of fiber pinhole and binning (schematic for demonstration purposes only; actual fiber count is 50, and pixel count is 256 rows and 1024 columns). Right: actual spectra obtained for a $Co_3O_4$ sample for signal fiber, background fibers, and the subtraction of the two. (d) Left: photograph of raster scanning hardware with components labeled. Inset shows the actual rastering pattern adopted for experiments. Right: comparison of spectra obtained with raster on (blue) and raster off (red) on a sample of $Co_3O_4$ at 185°C (baseline subtraction applied). [Colour figure can be viewed at wileyonlinelibrary.com]

microwave heating are more difficult to verify; if present, they were not severe enough to prevent adequate collection.

The collimated signal beam returns back through the dichroic and a low pass edge filter (Teledyne Princeton Instruments). The signal beam is then focused by a precision Z-axis adjustable aspheric (Teledyne Princeton Instruments) onto the bare termination of a fiber optic bundle (50–50 μm fibers, Teledyne Princeton Instruments), which is affixed in a precision XY stage (CP1XY, Thorlabs). In the current design, the optical aperture is 10 mm giving an N.A. of 0.033 with the objective lens focal length of 150 mm used. This could be readily increased to ~23 mm (N.A. 0.077) for more efficient collection by increasing the size of the probe's top opening and following optics.

The lens and the fiber termination stage were manually adjusted to focus the collimated signal beam onto a single fiber in the circular bundle (Figure 2c) The fiber bundle output to the spectrometer is vertically linearized with respect to the dispersive grating and charge-coupled device (CCD) detector camera. When the signal beam is focused on a single fiber, this arrangement creates a confocal "fiber pinhole" arrangement, which effectively reduces collection of any radiation surrounding the laser spot from thermal emission, from which no Raman scattering information would be collected. This proved essential for quality spectrum collection at high temperatures (>600°C) where thermal radiation and fluctuations become intense. The "signal" pixel rows (6) corresponding to laser-irradiated sample area and the remaining "background" pixel rows (219) corresponding to the non-irradiated area were binned separately and rescaled by their respective pixel counts. A baseline subtracted spectrum could then be obtained by subtracting the "background" from the "signal," removing many instrumental (non-laser induced) artifacts (Figure 2c, right plot). Conveniently, this baseline is collected (and not calculated) for each spectrum, and no adjustable parameters are necessary that could be difficult to optimize for the numerous spectra. For clarity, the baseline subtracted spectra were used to present the in situ data. This is not strictly necessary when background artifacts are irrelevant to the analysis; it will also not remove any laser induced artifacts such as sample fluorescence.

Laser-induced heating is an important consideration in Raman spectroscopy due to the necessity of using a highly focused laser spot. A useful feature of the fiber pinhole arrangement is the ability to compare the thermal background level (blackbody emission slope) of the "signal" spectrum to the "background" spectrum during the entire collection. The background collection area is not irradiated and should not undergo laser induced

heating. Therefore, an increased slope in the "signal" spectrum relative to the "background" spectrum will indicate clearly laser-induced heating is significant. When collecting on a stationary spot in dark opaque samples (e.g., $Co_3O_4$), significant heating due to the laser was observed. This is undesirable when attempting to representatively compare the effects of different heating methods. To address this, a simple custom mechanical raster scanning apparatus was designed to continuously move the probe (Figure 2d). An adjustable XYZ stage (XR25P/M and XR25-YZ/M, Thorlabs) supports the optical assembly, where manual adjustment of the Z-axis micrometer moves the entire assembly vertically for fine focusing on the sample before experiments are initiated. The X and Y stage micrometer drives were removed and replaced by screw drives and nuts (CNC Inc) actuated by microcontroller-controlled stepper motors (Nema 17, Longrunner) to allow rapid scanning movement of the assembly. An automated continuous orbital raster pattern was applied, which was 5 mm in total diameter. Each pattern cycle is completed in ~4.6 s. This effectively reduced laser-induced heating in $Co_3O_4$ samples (Figure 2d, right plot). Significant laser heating was not observed in anatase $TiO_2$ samples without rastering, even at elevated sample temperatures (>900°C), which may be due to the low intrinsic absorption of $TiO_2$ at the laser wavelength utilized.[42] For this study, though, rastering was still applied to reduce potential effects of laser heating during the conversion process. Rastering additionally provides a better bulk average analysis of the sample surface due to the small sampling volume. Minor variations in the area of sample surface selected may produce large spectral differences between sampling spots. By continuously moving during the collection, these discrepancies are avoided. Clearly, any heterogeneity in samples will be masked, and the spectra of components will be superimposed; therefore, the analysis will yield bulk transformation information only. If desired, a custom raster protocol for the purpose of Raman mapping could be readily deployed.

Conventional (furnace) heating experiments were performed with a small tube furnace (Superthal Mini MS 31, Kanthal) placed inside the microwave cavity, allowing measurements without moving or changing the instrument (Figure 3). The furnace was controlled using a proportional-integral-derivative (PID) temperature controller (3216, Eurotherm) and power controller (uF1HX-TA0-16-L1000, Control Concepts) modulated by a "furnace thermocouple" (Type B, Carbolite) inserted into the center of the furnace. A calibration of the furnace setting to the temperature measured by the "sample thermocouple" (Type K, PerfectPrime) was performed (Figure S1) to achieve the desired sample temperature.

Microwave experiments were performed using an insulation housing composed of aluminosilicate firebricks (Lynn Manufacturing) without any other

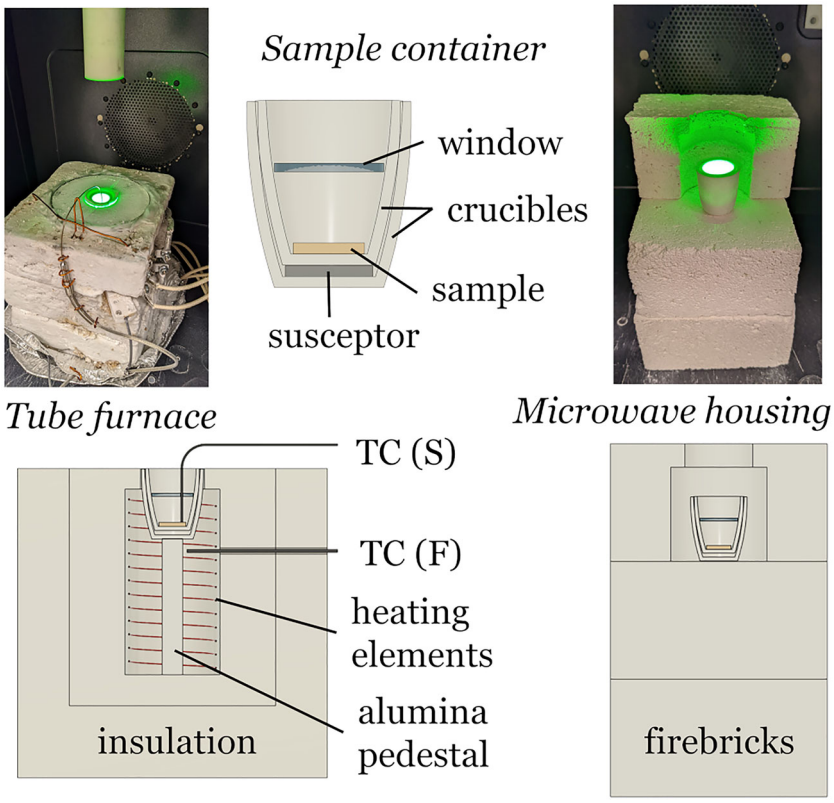


**FIGURE 3** Top left: photograph of tube furnace. Bottom left: cross-section schematic of tube furnace. Top middle: sample container schematic. Top right: photograph of microwave housing. Firebrick partially removed at top of housing to reveal sample container. Bottom left: cross-section schematic of microwave housing [Colour figure can be viewed at wileyonlinelibrary.com]

modifications to the instrument. These were stacked to place the sample approximately in the center of the microwave cavity. In the top firebrick housing, a 50 mm diameter hole was drilled partway to create an enclosure, which did not contact the sample/susceptor container. A smaller 38 mm diameter hole was drilled the rest of the way to provide optical access to the top surface of the sample by the Raman probe (Figure 3).

In both heating methods, the sample container consisted of an alumina "sample" crucible (AL-1005, Advalue Technology) nested inside a larger "susceptor" crucible (AL-1010, Advalue Technology), forming a flush semi-seal around the rim but with an open space beneath the sample crucible (Figure 3). For microwave experiments, this was filled with a secondary microwave susceptor material, namely, 3 g of natural $Fe_3O_4$ (94%, Alpha Chemicals). This was necessary to initiate heating as $TiO_2$ does not intrinsically heat efficiently under 2.45 GHz microwave irradiation at room temperature.[43] $Fe_3O_4$ was chosen as the susceptor as it heats rapidly[4] and does not release particulates (i.e., smoke) upon heating, which would interfere with the optical path for Raman collection. A custom quartz optical window (Advalue Technology) with a diameter of 20 mm formed a loose seal within the sample crucible to retain heat while still allowing a clear optical path for Raman collections.

In furnace experiments, the susceptor crucible was instead filled with SiC powder (Alfa Aesar) used only as a thermal transfer medium. These crucibles were supported by an alumina pedestal inside the furnace, forming a flush semi-seal between the furnace insulation opening and the crucibles at the top of the tube furnace. The temperature of the sample surface was measured by securing the "sample thermocouple" firmly onto the top of the sample and slightly outside of the laser scanning pattern. The temperature data were collected by computer using a USB temperature input device (USB-TC01, NI). In furnace experiments, a similar 20 mm diameter quartz window was employed (Advalue Technology). This window however had a 1.2 mm diameter through hole located 4.5 mm from the center of the window to allow insertion of the thermocouple and placement atop the sample.

## 3 | METHODS

The conventional furnace experiment was performed by increasing the temperature of the furnace at the maximum rate achievable. This resulted in a maximum heating rate of ~25°C/min measured at the sample surface. The temperature was held at ~855°C for ~1 h then allowed to cool naturally. The microwave experiment was performed by applying a constant power of 400 W for 40 min, after which the sample was allowed to cool naturally.

For each experiment, 0.5 g −325 mesh $TiO_2$ powder (> 99%, Sigma Aldrich) with 1 mol% of nanoparticulate CuO (added to lower the transition temperature and time) was homogenized by grinding in an agate mortar and pressing into 13 mm diameter circular pellets (18 MPa, 1 minute). The nanoparticulate CuO was prepared by a precipitation method adapted from a previous report.[44] Briefly, CuO (>99%, Sigma Aldrich) powder was dissolved in 3M HCl (VWR) followed by precipitating with 3M NaOH (Fisher Chemical). The product was washed by repeated suspension in DI water and centrifugation (5 × 100 ml) followed by drying at 100°C. All preparations and phase transformations were performed in ambient air.

The spectrometer (FER-SCI-1024B X-VR, Teledyne Princeton Instruments) is equipped with a 1200 g/mm grating (500 nm blaze) and a 1024 × 256 (w. by h.) pixel back-illuminated CCD detector cooled to −55°C. It provides spectral resolution of at least 0.13 nm (~4 $cm^{-1}$). The laser head power was fixed at 50 mW (50%) for all experiments. Spectra collection, temperature collection, and raster scanning were synchronously implemented by computer control using MATLAB. One spectrum per second was collected with 490 ms total camera exposure time per spectrum. Post collection, 10 spectra were averaged to avoid periodic changes that could arise from the rastering pattern. No further smoothing was applied in the presented data. Details of these instrument control and data analysis programs are described in the Supporting Information.

## 4 | RESULTS AND DISCUSSION

To demonstrate the utility of the new Raman probe for high-temperature studies under nonconventional (microwave) and conventional (furnace) heating conditions, observations of the irreversible anatase-to-rutile phase transition in $TiO_2$ are presented. The temperature/pressure phase diagram of $TiO_2$ polymorphs[45] suggests this conversion will occur above 600°C at ambient pressure. Reported temperatures of the transition vary from 600 to 1200°C and depend strongly on the size, microstructuring, preparation method, atmosphere, additives, and impurities.[40] In this work, microcrystalline anatase was used with 1 mol% nanoparticulate CuO added, and the transformation was performed in air. The CuO additive lowers the temperature and increases the rate of the transformation,[46] which was necessary to detect the

phase transformation at the temperatures employed. Due to the excitation wavelength used (532 nm), the Stokes Raman signals (collected at 533–555 nm) are masked by the intensity and fluctuations of thermal radiation at temperatures > 900°C (see Yashima et al.[47]). Pure microcrystalline anatase does not undergo the phase transition at time scales <1 day until temperatures exceeding ~1000°C are achieved, necessitating the use of the CuO additive.

Two experiments were performed to demonstrate the observation of the phase transition under both conventional (furnace) and microwave heating. Six Raman active modes in anatase before heating and four Raman active modes in rutile after heating are clearly identified (Figures S2 and S3) and are in good agreement with those previously reported.[48] No Raman signals were observed for the 1 mol% CuO additive. The spectra of rutile derived from both heating methods differed only slightly in their intensity profiles (Figure S4), which is likely due to slightly differing optical conditions. The rutile spectra were obtained from the surface of the sample pellet before homogenizing. Subsequent grinding and analysis by X-ray powder diffraction confirmed full conversion through the entire sample and no detectable side phases (Figure S5). This suggests that for this conversion process, Raman spectroscopic monitoring of the surface is a good indicator of transformation completion. This may not be the case for all systems, especially those where surface reactivity differs significantly from that of the bulk, and so conclusions of transformations should be confirmed by post-experiment homogenizing and analysis.

Presented are the Raman intensity surfaces and the phases that could be identified by analysis of the individual spectra (Figure 4). As can be observed, the dominant phases during the heating process could be clearly distinguished.

To estimate the outer bounds of the phase transition (initiation and completion), the evolution of the integrated peak area for selected Raman bands as the phase transition occurs was examined. For this procedure, the integrated area under a selected range of pixels (wavenumbers) for each peak was tracked over a limited time window encompassing the approach and recession of the transition. These selections are summarized in Tables S1 and S2. There is an obvious inflection point in the time dependence of the Raman peak integrated areas where the anatase peaks disappear and the rutile peaks appear. Using a linear change-point analysis method,[49,50] an initiation and completion time of the phase transitions could be estimated (Figures S6 and S8). While there are many possible methods to estimate phase transition time bounds, this procedure is simple and yields an objective approximation. The individual spectra before, during, and after the transition show visually that the procedure determined the detectable single- and multiphase regions sufficiently.

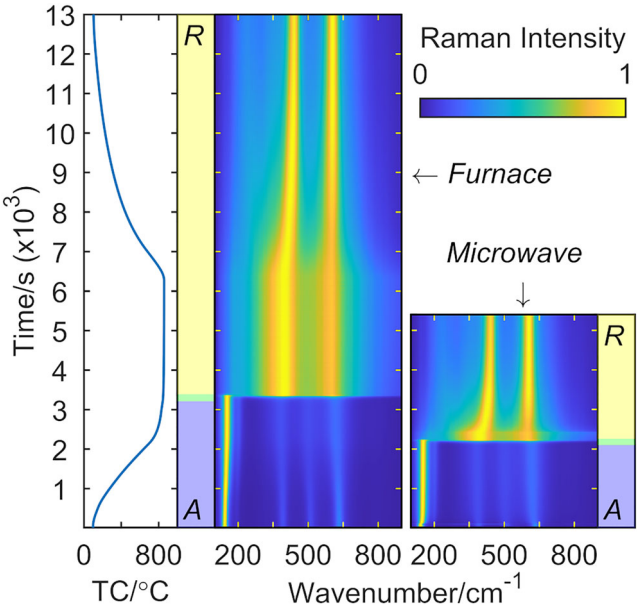


**FIGURE 4** Left plots (*Furnace*): temperature profile measured by sample thermocouple and Raman intensity surface plot of the transition performed under furnace heating. Dominant phases identified in the Raman spectra are indicated in the center bar ($A$ = anatase, blue; $R$ = rutile, yellow; mixture of phases indicated by green area between the two). Right plot (*Microwave*): Raman intensity surface plot of the transition performed under microwave heating on the same time scale as the furnace experiment. Dominant phases indicated in the right bar as in the furnace experiment. Note: The temperature profile measured by thermocouple (TC) at left was recorded only for the furnace experiment and does not apply to the microwave experiment. [Colour figure can be viewed at wileyonlinelibrary.com]

Three of the four most prominent anatase Raman modes (143, 506, and 632 $cm^{-1}$, denoted by their peak positions measured at 100°C) yielded consistent transition initiation times, which were averaged. The other mode at 388 $cm^{-1}$ was not consistent, likely due to the overlap with the appearing rutile peaks. The two most prominent rutile Raman modes (393 and 592 $cm^{-1}$, measured at 100°C) gave close transition completion times and were likewise averaged. It is likely the actual transition process extends somewhat beyond these bounds and should not be taken to be a perfect representation; for example, a slight indication of anatase phase persisting beyond the determined transition completion time can be observed (Figures S7 and S9). A limitation of phase evolution tracking by Raman spectroscopy is weak signals from the minority phase being indistinguishable from stronger signals of the dominant phase due to overlap. This procedure should therefore not be taken as perfectly

analytical; still, it has clear utility in qualitatively comparing different heating methods with respect to the time taken to fully complete the transformation and does not rely on subjective visual inspection.

Under conventional heating, the transition takes approximately 180 s to complete. The temperatures measured at the surface by thermocouple give an initiation temperature of 843°C and a completion temperature of 849°C. Under microwave heating, the estimated time is only slightly reduced to 160 s. Therefore, significant changes in the transition process time scale under microwave heating are not supported.

It should be noted that temperature was not measured under microwave heating. Accurate temperature measurement during microwave heating processes presents great challenges and is still a largely unsolved problem. Thermocouples should be avoided (they are typically metallic and couple with the microwave radiation),[51] and achieving accuracy by pyrometry methods is complex.[27] Some temperature profile information may be derived from tracking of the Raman peak position during the heating process as these are known to shift predictably with temperature due to anharmonicity.[32,33] The peak position of the main anatase band (143 $cm^{-1}$) shifts to higher wavenumber values with increasing temperature, and a strong correlation to the temperature measured by the sample thermocouple in the furnace experiment was observed (Figure S10). Tracking of the shift of this band position in the microwave experiment indicates an extremely rapid initial heating rate followed by a drawn out, more gradual heating rate period approaching the phase transition. This suggests that temperature is not likely a strong factor in impacting the transition process time scales between the furnace and microwave heating method presented and is supported by the similar time scales revealed by the Raman analysis. Analytical temperature measurement is essential for further comparison of the heating methods, and the realization of this is part of our ongoing work. Still, the in situ Raman data collected clearly show the time to achieve full conversion is reduced (furnace: 57 min, microwave: 38 min) presumably due to higher heating rates achieved in microwave reactors.

## 5 | CONCLUSIONS

An in situ Raman measurement system was developed for the monitoring and direct comparison of solid-state transformations under conventional (furnace) heating and nonconventional microwave heating. A custom designed microwave compatible Raman probe capable of measuring inside commercially available, general-use laboratory microwave ovens is integrated into an in situ Raman measurement system. The high-temperature phase transition of $TiO_2$ from anatase to rutile was observed under furnace and microwave heating conditions at temperatures exceeding 800°C. The newly developed measurement system could eventually enable comparison of conventional and microwave methods for high-temperature, solid-state transformations. This will provide an additional useful tool for understanding and controlling microwave processing of inorganic materials, especially in routine syntheses in the laboratory setting.

## ACKNOWLEDGEMENT

This work was funded in part by the Deutsche Forschungsgemeinschaft (456639820). The material is based upon work supported by the National Science Foundation under grant number 2143982. We gratefully acknowledge Dr. Emmanuel Soignard for helpful advice in the design of the instrument. Open Access funding enabled and organized by Projekt DEAL.

## ORCID

*Christina S. Birkel* https://orcid.org/0000-0001-8979-5214

## REFERENCES

[1] H. J. Kitchen, S. R. Vallance, J. L. Kennedy, N. Tapia-Ruiz, L. Carassiti, A. Harrison, A. G. Whittaker, T. D. Drysdale, S. W. Kingman, D. H. Gregory, *Chem. Rev.* **2014**, *114*, 1170.
[2] E. E. Levin, J. H. Grebenkemper, T. M. Pollock, R. Seshadri, *Chem. Mater.* **2019**, *31*, 7151.
[3] J. P. Siebert, C. M. Hamm, C. S. Birkel, *Appl. Phys. Rev.* **2019**, *6*, 041314.
[4] K. J. Rao, B. Vaidhyanathan, M. Ganguli, P. A. Ramakrishnan, *Chem. Mater.* **1999**, *11*, 882.
[5] D. M. P. Mingos, D. R. Baghurst, *Chem. Soc. Rev.* **1991**, *20*, 1.
[6] D. R. Baghurst, A. M. Chippindale, D. M. P. Mingos, *Nature* **1988**, *332*, 311.
[7] H. X. Yang, C. J. Nie, Y. G. Shi, H. C. Yu, S. Ding, Y. L. Liu, D. Wu, N. L. Wang, J. Q. Li, *Solid State Commun.* **2005**, *134*, 403.
[8] V. Subramanian, C. L. Chen, H. S. Chou, G. T. K. Fey, *J. Mater. Chem.* **2001**, *11*, 3348.
[9] M. Nakayama, K. Watanabe, H. Ikuta, Y. Uchimoto, M. Wakihara, *Solid State Ionics* **2003**, *164*, 35.
[10] C. Mastrovito, J. W. Lekse, J. A. Aitken, *J. Solid State Chem.* **2007**, *180*, 3262.
[11] J. W. Lekse, A. M. Pischera, J. A. Aitken, *Mater. Res. Bull.* **2007**, *42*, 395.
[12] J. W. Lekse, T. J. Stagger, J. A. Aitken, *Chem. Mater.* **2007**, *19*, 3601.
[13] K. Biswas, S. Muir, M. A. Subramanian, *Mater. Res. Bull.* **2011**, *46*, 2288.
[14] S. W. Muir, O. D. Rachdi, M. A. Subramanian, *Mater. Res. Bull.* **2012**, *47*, 798.
[15] D. K. Agrawal, *Curr. Opin. Solid State Mater. Sci.* **1998**, *3*, 480.
[16] J. D. Katz, *Annu. Rev. Mater. Sci.* **1992**, *22*, 153.

[17] B. Panzarella, G. Tompsett, W. C. Conner, K. Jones, *ChemPhysChem* **2007**, *8*, 357.
[18] G. A. Tompsett, B. Panzarella, W. C. Conner, K. S. Yngvesson, F. Lu, S. L. Suib, K. W. Jones, S. Bennett, *Rev. Sci. Instrum.* **2006**, *77*, 124101.
[19] D. S. Wragg, P. J. Byrne, G. Giriat, B. Le Ouay, R. Gyepes, A. Harrison, A. G. Whittaker, R. E. Morris, *J. Phys. Chem. C* **2009**, *113*, 20553.
[20] S. Vaucher, R. Nicula, J. M. Català-Civera, B. Schmitt, B. Patterson, *J. Mater. Res.* **2008**, *23*, 170.
[21] S. Vaucher, M. Stir, K. Ishizaki, J. M. Catala-Civera, R. Nicula, *Thermochim. Acta* **2011**, *522*, 151.
[22] G. R. Robb, A. Harrison, A. G. Whittaker, *PhysChemComm.* **2002**, *5*, 135.
[23] A. G. Whittaker, A. Harrison, G. S. Oakley, I. D. Youngson, R. K. Heenan, S. M. King, *Rev. Sci. Instrum.* **2001**, *72*, 173.
[24] A. Harrison, R. Ibberson, G. Robb, G. Whittaker, C. Wilson, D. Youngson, *Faraday Discuss.* **2003**, *122*, 363.
[25] M. M. Günter, C. Korte, G. Brunauer, H. Boysen, M. Lerch, E. Suard, *Zeitschrift Anorg. Und Allg. Chemie.* **2005**, *631*, 1277.
[26] B. Garcia-Baños, J. Catalá-Civera, F. Peñaranda-Foix, P. Plaza-González, G. Llorens-Vallés, *Materials.* **2016**, *9*, 349.
[27] S. Vaucher, J.-M. Catala-Civera, A. Sarua, J. Pomeroy, M. Kuball, *J. Appl. Phys.* **2006**, *99*, 113505.
[28] B. García-Baños, J. J. Reinosa, F. L. Peñaranda-Foix, J. F. Fernández, J. M. Catalá-Civera, *Sci. Rep.* **2019**, *9*, 10809.
[29] J. M. Catala-Civera, A. J. Canos, P. Plaza-Gonzalez, J. D. Gutierrez, B. Garcia-Banos, F. L. Penaranda-Foix, *IEEE Trans. Microw. Theory Tech.* **2015**, *63*, 2905.
[30] E. Smith, G. Dent, *Modern Raman spectroscopy - a practical approach*, John Wiley & Sons, Ltd, Chichester **2005**.
[31] J. Thapa, B. Liu, S. D. Woodruff, B. T. Chorpening, M. P. Buric, *Appl. Opt.* **2017**, *56*, 8598.
[32] T. R. Hart, R. L. Aggarwal, B. Lax, *Phys. Rev. B* **1970**, *1*, 638.
[33] J. Menéndez, M. Cardona, *Phys. Rev. B* **1984**, *29*, 2051.
[34] P. Mishra, K. P. Jain, *Phys. Rev. B* **2000**, *62*, 14790.
[35] S. Osswald, V. N. Mochalin, M. Havel, G. Yushin, Y. Gogotsi, *Phys. Rev. B* **2009**, *80*, 075419.
[36] G. Gouadec, P. Colomban, *Prog. Cryst. Growth Charact. Mater.* **2007**, *53*, 1.
[37] S. Sandell, E. Chávez-Ángel, A. El Sachat, J. He, C. M. Sotomayor Torres, J. Maire, *J. Appl. Phys.* **2020**, *128*, 131101.
[38] R. Merlin, A. Pinczuk, W. H. Weber, *Overview of phonon Raman scattering in solids*, Springer, Berlin **2000**.
[39] T. M. Devine, F. Adar, *Characterization of materials*, John Wiley & Sons, Inc., Hoboken **2012** 1.
[40] D. A. H. Hanaor, C. C. Sorrell, *J. Mater. Sci.* **2011**, *46*, 855.
[41] Alumina 99.9% - 100%|CoorsTek Technical Ceramics. https://www.coorstek.com/en/materials/technical-ceramics/alumina/alumina-999-100/, (accessed 30 May 2022).
[42] J. Yao, Z. Fan, Y. Jin, Y. Zhao, H. He, J. Shao, *Thin Solid Films* **2008**, *516*, 1237.
[43] D. R. Baghurst, D. M. P. Mingos, *J. Chem. Soc., Chem. Commun.* **1988**, 829.
[44] K. Phiwdang, S. Suphankij, W. Mekprasart, W. Pecharapa, *Energy Procedia.* **2013**, *34*, 740.
[45] J. C. Jamieson, B. Olinger, *Am. Mineral.* **1969**, *54*, 1477.
[46] R. D. Shannon, J. A. Pask, *J. Am. Ceram. Soc.* **1965**, *48*, 391.
[47] M. Yashima, M. Kakihana, R. Shimidzu, H. Fujimori, M. Yoshimura, *Appl. Spectrosc.* **1997**, *51*, 1224.
[48] U. Balachandran, N. G. Eror, *J. Solid State Chem.* **1982**, *42*, 276.
[49] R. Killick, P. Fearnhead, I. A. Eckley, *J. Am. Stat. Assoc.* **2012**, *107*, 1590.
[50] M. Lavielle, *Signal Process.* **2005**, *85*, 1501.
[51] E. Pert, Y. Carmel, A. Birnboim, T. Olorunyolemi, D. Gershon, J. Calame, I. K. Lloyd, O. C. Wilson, *J. Am. Ceram. Soc.* **2001**, *84*, 1981.

## SUPPORTING INFORMATION

Additional supporting information can be found online in the Supporting Information section at the end of this article.

**How to cite this article:** J. Jamboretz, A. Reitz, C. S. Birkel, *J Raman Spectrosc* **2023**, *54*(3), 296. https://doi.org/10.1002/jrs.6478